AIMS Materials Science, 2(4): 379-391.
DOI: 10.3934/matersci.2015.4.379
Received date 03 June 2015,
Accepted date 27 September 2015,
Published date 16 October 2015

http://www.aimspress.com/

Research article

Diversity of internal structures in inhibited epoxy primers

Anthony E. Hughes [1,2], Y. Sam Yang [3,*], Simon G. Hardin [4], Andrew Tulloh [3], Yudan Wang [5], and You He[5]

[1] Institute for Frontier Materials, Deakin University, Waurn Ponds 3216 Victoria Australia
[2] CSIRO, Mineral Resources, Clayton 3169, Victoria, Australia
[3] CSIRO, Manufacturing, Private Bag 10, Clayton 3169 Victoria Australia
[4] School of Chemistry, University of Melbourne, Parkville 3010 Victoria Australia
[5] Shanghai Institute of Applied Physics, Chinese Academy of Sciences, Shanghai, P. R. China

* **Correspondence:** Email: sam.yang@csiro.au; Tel: +61-3-9545-2759;
Fax: +61-3-9544-1128.

Abstract: Computed tomography is making a significant impact in the field of materials science in recent years. In this paper the authors report on advances made in three areas of characterization and also identified where further research needs to be focused. First we report on a new approach to data analysis called "Data Constrained Modelling (DCM)" in which compositional tomography can be undertaken rather than adsorption or phase contrast tomography. This is achieved by collecting X-ray CT data at different energies and then combining the datasets to reconstruct 3D compositional tomography. Second, on the application of this approach to inhibited primers typical of those used in the aerospace industry. Aerospace primers are effectively composite materials containing inorganic phases which are bound together with a polymer. Understanding the materials science of these systems requires information over several orders of magnitude in length-scale. In this paper we report on how DCM can be used to extend our understanding at the smaller length scales at the limits of resolution of the technique. The third and final advance is in extending the approach to include 4-dimensional studies. In this case we examine the primer before and after leaching. This process causes changes in the primer which can be both detected and quantified using the above approach.

Keywords: computed tomography; data constrained modeling; inhibited primers; chromate inhibitors; x-ray absorption tomography

1. Introduction

There are many materials encountered where one may have a phenomenological understanding of the properties, but no real fundamental understanding of the structure. Epoxy coatings, particularly high performance ones, are a good example of where 3D characterization has helped understand current coatings structure [1,2,3]. It has also guided research into new areas such as in self-healing coatings [4]. These advances are, in part, due to the depiction of the 3D structure and in part due to absorption contrast techniques, which reveal features that are not probed by other techniques such as density variation in the polymer itself [2].

For example, it has been shown that strontium chromate ($SrCrO_4$) inhibitor particles in high performance aerospace coatings form clusters of particles that extend throughout the coating [1,2]. Tomography studies have allowed for the determination of the cluster size distributions and have shown that the clusters have fractal dimensions, this information is important for understanding the transport of inhibitors and corrodents. Thus the presence of these clusters explained anomalies in the leaching characteristics of the $SrCrO_4$ characterized by very fast initial release, which slowed to zero release over time (typically one to two weeks) even though there was still considerable $SrCrO_4$ remaining in the coating. This behavior was attributed to cluster formation, where leaching only came from $SrCrO_4$ clusters connected to the external environment. The release began with direct dissolution into electrolyte followed by a period where release was dominated by the fractal nature of the cluster size and shape (fractal) and finally slowed to zero when all the $SrCrO_4$ in the cluster was fully dissolved. The same studies also revealed that there were "density" differences within the polymer. The origin of these differences is still the subject of intense study, but it was proposed that polymerization of the epoxy resin occurred preferentially on the $SrCrO_4$ particles expelling solvent into the space between the $SrCrO_4$ particles and clusters and reducing the atom number density for the remaining polymerization.

The characterization and processes described above, occur on a range of scales from tens of microns down to the nanoscale which represents a challenge for X-ray CT techniques, although it has been used widely together with image segmentation [5,6]. The study of these systems presents further challenges in distinguishing different chemicals within these systems as well as with feature registration for following changes with time such as the leaching of inhibitors. The development of the DCM approach [7,8–12] to study these systems has considerably enhanced the extraction of the chemical information as demonstrated below. Sample registration for before and after leaching is an ongoing issue, particularly as length scales become smaller. In this paper, the DCM approach is described for an epoxy-based system containing a TiO_2 pigment along with $SrCrO_4$ inhibitor.

2. Materials and Methods

2.1. Sample Preparation

2.1.1. Sample Preparation

The sample was cast in a cylindrical geometry (Figure 1), and was prepared using commercially obtained materials. The inhibitor $SrCrO_4$ (Sigma Aldrich) and filler, rutile, TiO_2, (Sigma Aldrich)

were used as the solid phases. Inhibitor and pigment were dispersed in 2-part Struers Epofix according to the manufacturer's specifications. The composition of the mixture was 10% w/w each of inhibitor and pigment and 80% w/w polymer. Polyethylene (PE) tubing of 1500μ inner diameter was fitted over a syringe, and the sample drawn into the tubing by suction. The tubing was then sealed with a clamp at one end. The tubing was mounted vertically with the sealed end at the bottom, and the top open, to facilitate escape of air bubbles, and the sample allowed to cure at room temperature overnight. The sample was then cut to about lengths around 5mm, and the tubing removed with a scalpel blade. The sample chosen was mounted in a plastic mounting tip with Superglue®. After CT data acquisition, the same sample was immersed in 0.1 M HCl (pH 1.0) for 2 days at ambient temperature, then rinsed by immersion in de-ionized water overnight. The sample was dried in air at ambient temperature for several hours before acquisition of the post-leaching CT data.

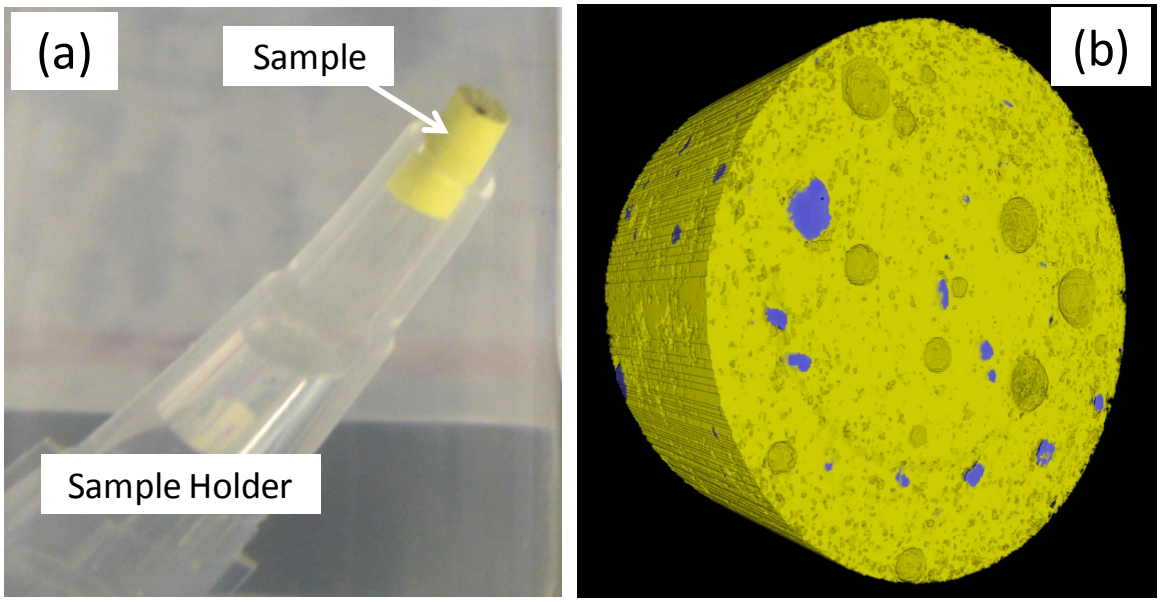

Figure 1. The sample, consisting of $SrCrO_4$ and TiO_2 mixed into an epoxy, was prepared in the form of cylinder with a diameter of 1500 μm as depicted in (a). In this instance the sample, is mounted in the examination holder. (b) The 3D reconstruction shows $SrCrO_4$ particles in blue and the epoxy in yellow. The circular features are dimples created by air bubbles in the epoxy and the mottling is lower density epoxy.

2.1.2. Synchrotron-based X-ray CT

X-ray CT was performed at the Shanghai Synchrotron Radiation Facility (SSRF) BL13W imaging beam-line. A 2x optical lens was employed to achieve an effective pixel size of 3.7 μm. Before leaching, 2 data sets were acquired at X-ray beam energies at 15 keV and 18 keV respectively. After leaching another 2 data sets were acquired with the same imaging parameters. For each dataset a total of 900 projection images was collected with a total sample rotation angle of 180°. Five flat-field

images were collected before and after the projection images respectively, and five dark-field images were collected after the completion of the projections.

The CT slices were reconstructed with the X-TRACT software by using the method of filtered back-projection of parallel X-ray beams [13]. Background corrections were applied using an average flat-field and an average dark-field image. Paganin's phase-retrieval algorithm was applied with parameters tuned to optimize the signal-to-noise ratio and minimize the edge enhancement without loss of resolution [14]. Ring artefacts were corrected using a polar coordinate transformation. The two reconstructed CT data sets prior to leaching at different energies was translated and rotated to maximize the cross-correlation. The same alignment procedure was applied to the post-leaching data sets. Each data set consisted of cubic voxels of $3.7\times3.7\times3.7\,\mu m^3$ on a 3D simple-cubic lattice. The following 3D analysis is based on such a 3D lattice.

3. Results

3.1. DCM approach

For a voxel at n ($n=1,2,\cdots,N$) where N is the total number of voxels in the system, and denoting $v_n^{(m)}$ ($m=0,1,2,\cdots,M$) as the volume fraction for material composition m in the voxel, the difference between the expected and CT reconstructed linear absorption coefficient is expressed as [15]

$$\Delta\mu_n^{(l)}=\sum_{m=1}^{M}\mu^{(l,m)}v_n^{(m)}-\overline{\mu}_n^{(l)}\qquad l=1,2,\cdots,L \tag{1}$$

Where L is the total number of CT data sets taken at different X-ray beam energies. $\mu^{(m,l)}$ is the total linear absorption coefficient for material m taken at X-ray energy l, and $\overline{\mu}_n^{(l)}$ is the CT reconstructed linear absorption coefficient at X-ray energy l.

The linearized phenomenological energy is expressed as

$$E_n=-\sum_{m=0}^{M}S^{(m)}v_n^{(m)}-\sum_{k=0}^{K}\sum_{j=1}^{N^{(k)}}\sum_{m=0}^{M}\sum_{m'=0}^{M}I_k^{(m,m')}\widetilde{v}_{n+n_j^{(k)}}^{(m')}v_n^{(m)} \tag{2}$$

In the above, the 1st term is the self-energy. A positive self-energy $S^{(m)}$ will decrease the volume fraction for composition m and a negative value will have the opposite effect. The symbol $\widetilde{v}_{n+n_j^{(k)}}^{(m')}$ represents the initial volume fraction for composition m'. In numerical terms, it is the value after the last iteration. The 2nd term with $k=0$ ($k>0$) accounts for the effect of interactions among compositions in the same voxel (with the neighbouring voxels). The factor $I_k^{(m,m')}$ is the interaction

between compositions m and m' at a neighbouring distance k. The maximum neighbouring distance is K. The number of neighbouring voxels with neighbour distance k is denoted as $N^{(k)}$ and the j'th neighbouring vector with a neighbouring distance k is denoted by $n_j^{(k)}$. A negative $I_k^{(m,m')}$ value models attractive interaction between compositions m and m' and a positive value has the opposite effect.

The solution to the problem is obtained by varying the material volume fractions such as to minimize the value of $\left|\Delta\mu_n^{(l)}\right|$ and E_n in Eqs. (1) and (2) [10,16]. It can be achieved by maximizing the following objective function:

$$T_n = -\sum_{m=0}^{M} S^{(m)} v_n^{(m)} - \sum_{k=0}^{K}\sum_{j=1}^{N^{(k)}}\sum_{m=0}^{M}\sum_{m'=0}^{M} I_k^{(m,m')} \tilde{v}_{n+n_j^{(k)}}^{(m')} v_n^{(m)} - \sum_{l=1}^{L} R^{(l)}\left[P_n^{(l)} + Q_n^{(l)}\right] \tag{3}$$

Subject to the following conditions

$$\begin{cases} 0 \le v_n^{(m)} \le 1 \\ \sum_{m=0}^{M} v_n^{(m)} = 1 & m = 0,1,2,\cdots,M; \quad n = 1,2,\cdots,N \\ P_n^{(l)}, Q_n^{(l)} \ge 0 \qquad l = 1,2,\cdots,L \end{cases} \tag{4}$$

The factor $R^{(l)}$ in the 3rd term of Equation (4) is the user specified weight factor relating to the significance of CT data error for beam energy l. A higher value would make it more sensitive to the data noise for the relevant beam energy. When the CT experimental error is small, for numerical simplicity and efficiency, $\left|\Delta\mu_n^{(l)}\right|$ can be treated as zero. The problem is further simplified if it is assumed that different compositions have the same self-energy so that the self-energy term can be ignored. In this article, the interactional term in the same voxel ($k = 0$) is ignored such that the model can be linearized to reduce computational complexity. For some cases, such simplifications can lead to satisfactory results [8,17]. For the samples studied in this paper, we have used $S^{(\text{void})} = 2$. All other parameters use default values for the DCM software [18]. That is $S^{(\text{epoxy})} = S^{(\text{SrCrO}_4)} = S^{(\text{TiO}_2)} = 0$; $R^{(15\text{keV})} = R^{(18\text{keV})} = 10$. All intra-voxel interaction energies take values of -1 for the same compositions, and all other interactions values are 0. Details about parameter selections have been published elsewhere [15,19].

3.2. Numerical results

Figure 1(b) is a reconstruction of a section of the cylindrical sample showing the epoxy in yellow and $SrCrO_4$ in blue. The sample was examined prior to and after the leaching experiment. It was evident, when comparing the sample prior to and after leaching, that while some $SrCrO_4$ particles have been dissolved a significant number of them are still present in the sample after leaching as discussed below.

The reason for only partial removal has been explained in previous studies where it was reported that $SrCrO_4$ formed independent clusters of particles and it was only those clusters connected to the external surface were dissolved. The algorithm for identifying clusters first interrogates voxels with shared faces, edges and corners then assigns them as either $SrCrO_4$ voxels or not. In the previous study many large extended clusters of $SrCrO_4$ were identified using this approach [1,2]. The clusters of $SrCrO_4$ voxels before and after leaching are presented in Figure 2. Unlike the extended clusters seen in the previous study, the clusters in Figure 2 appear to occupy isolated volumes within the polymer resin. In order to determine the fractal behaviour of the $SrCrO_4$ clusters and starting with a voxel as the origin near the centroid, a sequence of counting spheres with increasing diameters were used to count the number of voxels which belong to the cluster. The numbers of cluster voxels versus the counting sphere diameters are shown in Figure 3 for the largest cluster. As a reference, the numbers of the voxels in the counting sphere are also displayed (Figure 3). It is evident that, before leaching, $SrCrO_4$ forms compact 3D clusters. After leaching, the cluster become less compact. However, it does not show a clear fractal structure. The reason for this difference compared to the previous study is not clear but the presence of the TiO_2 and the mixing process are key parameters that should be assessed for their influence on the distribution or particles.

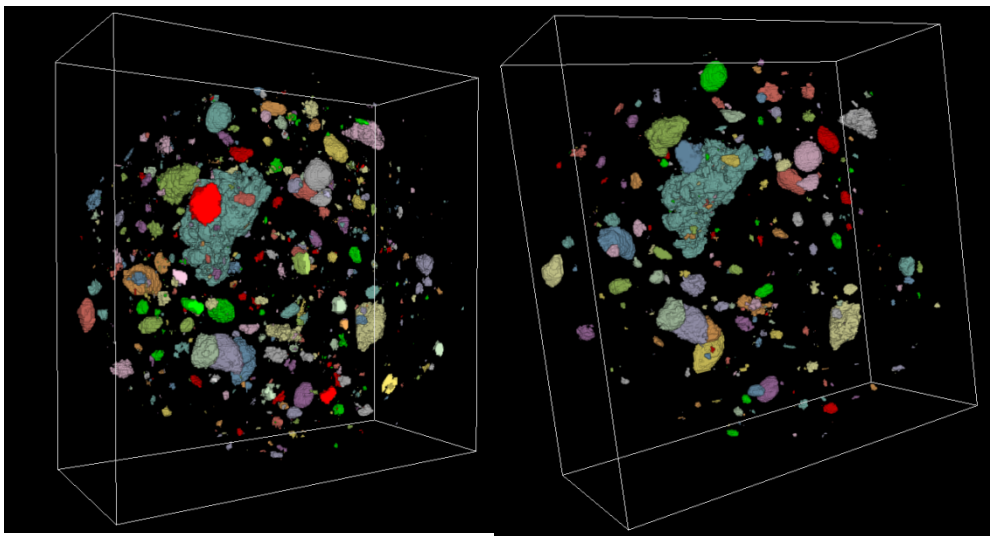

Before After

Figure 2. Rendering of the $SrCrO_4$ clusters before and after the leaching experiments. It can be seen that leaching reduces the volume and number of inhibitor particles.

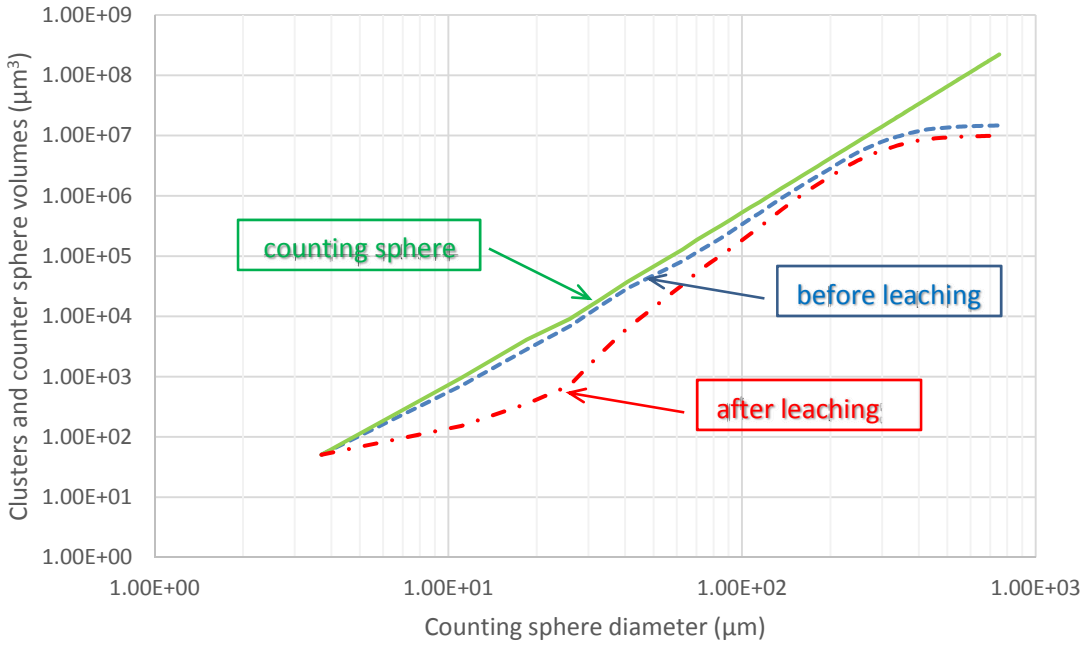

Figure 3. The total volume of voxels belonging to the largest $SrCrO_4$ cluster as a function of the counting sphere diameter. The centre of the counting sphere is at a voxel which belongs to the cluster and near the centroid of the cluster. The dashed line (blue) corresponds to the largest cluster before leaching, the dash-dot line (red) is for the largest cluster after leaching. As a reference, the solid line refers to the total volume of all voxels in the counting sphere.

It is clear from Figures 2 and 3, that $SrCrO_4$ particles have been dissolved from the sample. However, previous studies indicated that only the $SrCrO_4$ clusters connected to the external surface were the ones that were dissolved. The largest clusters in that study were 100 to 300 µm extended in the plane of the coating. They were also entangled and so the volume occupied by any individual (large) cluster increased with a fractal dimension of 2.3 to 2.5. In previous studies the release mechanism for CrO_4^{2-} was proposed to be via transport through the dissolving $SrCrO_4$ clusters since the chromate ion was too large to diffuse through the polymer network which had a molecular pore volume of 5.5Å according to positron annihilation lifetime measurements [20]. In this study it appears that $SrCrO_4$ particles in the body of the polymer have been dissolved without apparent connection via a dissolving $SrCrO_4$ network. The dissolution of apparently isolated $SrCrO_4$ particles/clusters from the centre of this sample suggests that a different leaching mechanism is at play which may be due to any or all of the following reasons which will be examined in more detail below. These include:

1. Alternative connected pathways via the TiO_2.
2. Molecular pore volume is larger in this sample allowing diffusion through the epoxy.
3. Alternative connected pathways via the epoxy such as through void or lower density epoxy.

The relationships between the size of the $SrCrO_4$ clusters and the numbers of such clusters before and after leaching are shown in Figure 4. On the logarithmic scale, they appear as linear when the logarithm for the number of clusters is squared. The correlation coefficients for linear fits to the data are good supporting a linear trend in the data. The curve for the leached sample shows fewer clusters

than that before leaching and the gradient is smaller than that before leaching. The intercept decreases from around 7.5 to 5.2 with leaching indicating that the largest cluster size is smaller after leaching. The difference between the two distributions is more obvious towards the origin of the horizontal axis. That is, it appears that a higher proportion of small $SrCrO_4$ clusters had been leached out.

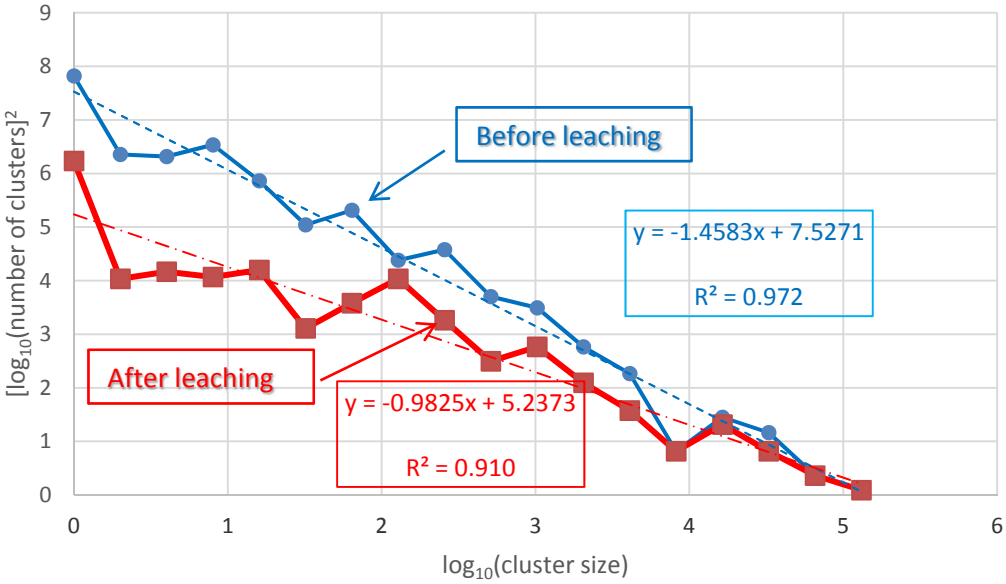

Figure 4. Relation between the size (number of voxels) and the number of the $SrCrO_4$ clusters.

The distribution of the TiO_2 (red) with respect to the $SrCrO_4$ (blue) is shown in Figure 5. The TiO_2 particles are much smaller on average than the $SrCrO_4$ particles and well dispersed within the sample. Moreover, by comparison to the $SrCrO_4$ particles there is no change in the distribution after the leaching experiment. The TiO_2 and $SrCrO_4$ clusters/particles were largely independent of each other *i.e.*, they do not have many points where they touch. Moreover even in the cases where this occurs the clusters that combine both TiO_2 and $SrCrO_4$ do not connect to the external surface. Therefore the interface between the TiO_2 particles and the epoxy apparently does not provide an alternative pathway through the polymer for the transport of dissolved $SrCrO_4$.

Figure 6 shows the distribution of void and low density epoxy (LDE). The LDE/void networks not connected to the external surface are presented in colour. For purpose of illustration of connectedness, an arbitrary voxel porosity value was set at 0.6. When the voxel porosities of two neighbouring voxels are both above 0.6, they are regarded as connected. These connected voxels were then labelled with the same colour and form extended volumes within the sample. The volumes not connected to the external surface appear in colours whereas all those volumes connected to the external surface are grey. The concentration of coloured volumes within the sample indicates that the void and LDE near the centre of the sample are less connected to the external surface before leaching. After leaching, the clusters that were previously disconnected from the external surface centre of the sample apparently become connected to the external surface through new pathways. This may be due to additional void voxels which are created during the leaching process via dissolution of $SrCrO_4$ particles.

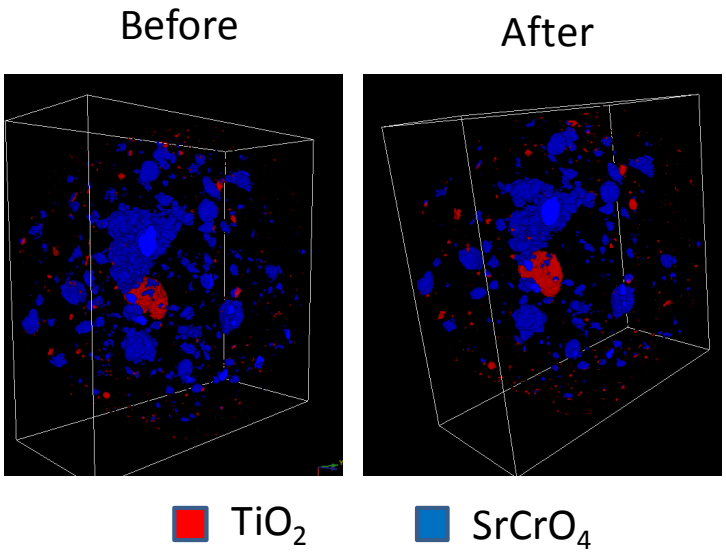

Figure 5. Distribution of TiO_2 (red) and $SrCrO_4$ (blue). In this instance all the $SrCrO_4$ cluster information has been removed and all particles are blue apart from the larger aggregation of TiO_2 voxels.

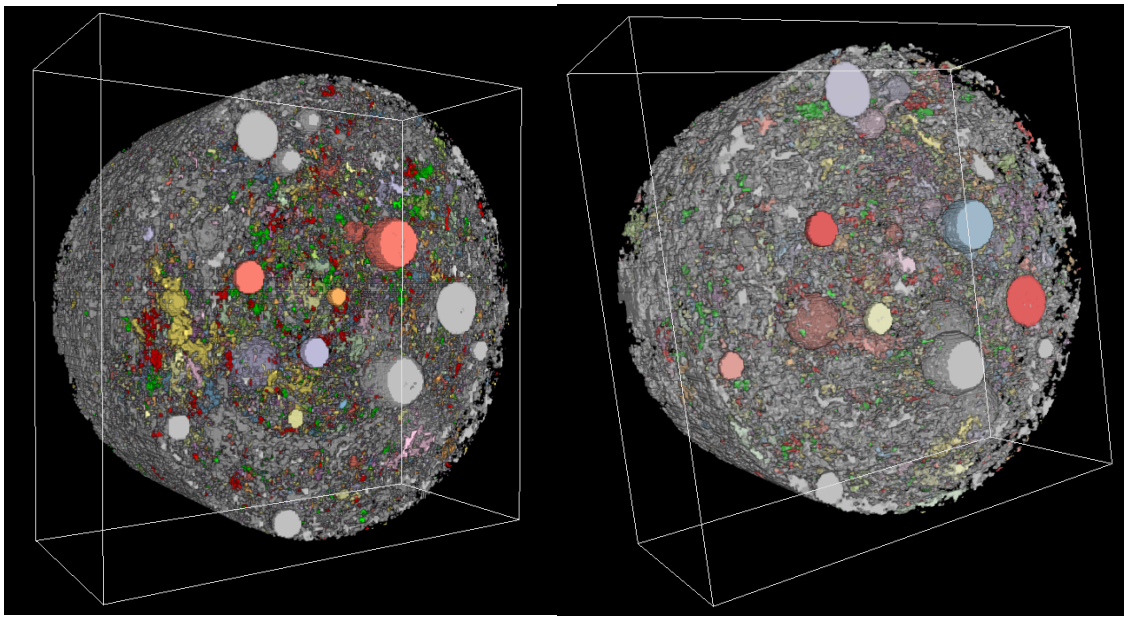

Figure 6. Connections of the combined void and low-density epoxy. An arbitrary threshold value of 0.6 voxel porosity is selected. Different colors represent different connected void/LDE clusters. The gray color represent voxels which are connected to the external surface.

Clearly this data shows that there are differentiated polymer networks within the sample in the form of LDE and voids. Whether these networks form pathways for the transport of chromate ions cannot be resolved from this study. However, if the molecular pore volume in this sample is similar to

that previously reported for this epoxy (5.5Å) then connected volumes of LDE and void may be the alternative pathway for the transport of chromate from within the epoxy to the external surface. The nature of this LDE component itself is unclear and may vary according to details of the monomer and cross-linker. Regions where there is a high level of cross-linking and a long cross-linking agent may have a lower density than regions with low cross-linking density where the polymer backbone is free to expand providing significant intermolecular free volume.

Similar to the largest $SrCrO_4$ cluster, fractal analysis has been performed for the largest void/LDE cluster before and after leaching, as shown in Figure 7. Obviously, the centroid of such a large void/LDE cluster is near the centre of the sample. The largest void/LDE cluster has a complicated structure as is shown in Figure 7 exhibiting a non-linear relationship between the counting sphere diameter and the voxels in the cluster suggesting no single fractal dimension. After leaching additional void/LDE voxels have been created as a result of dissolution of the $SrCrO_4$ resulting in a larger fractal dimension that approaches volumes of the sphere.

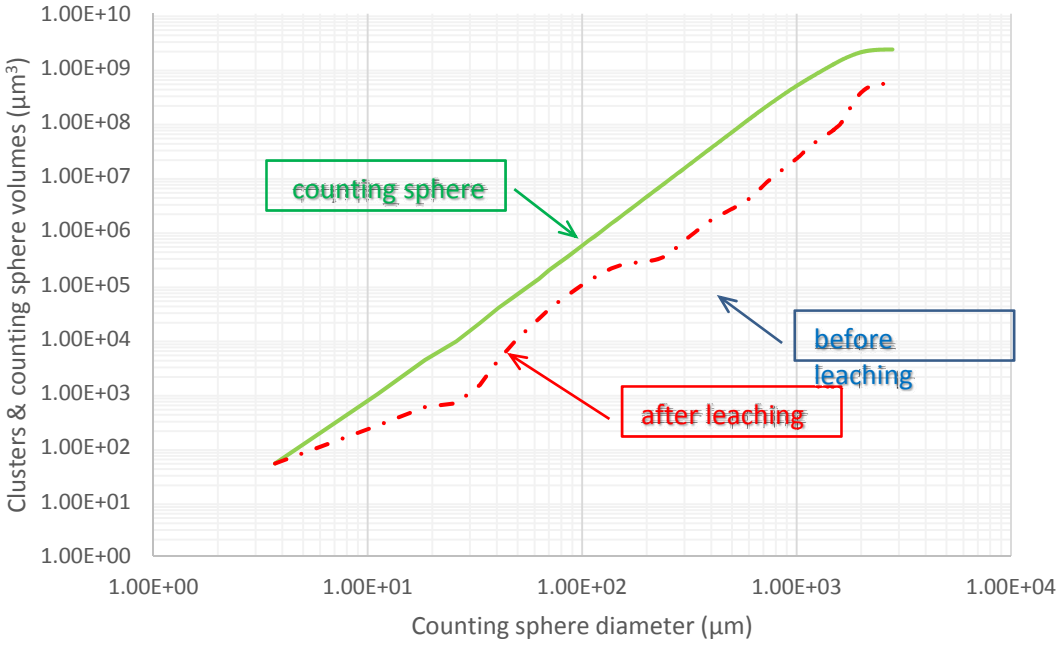

Figure 7. The total volume of voxels belongs to the largest void/LDE cluster as a function of the counting sphere diameters. The centre of the counting sphere is at a voxel which belongs to the cluster and near the centroid of the cluster. This is apparently near the centre of the sample. The dashed line (blue) corresponds to the largest cluster before leaching, the dash-dot (red) line is for the largest cluster after leaching. As a reference, the solid line refers to the total volume of all voxels in the counting spheres.

4. Discussion

The focus of this paper is on the leaching of inhibitor from an epoxy. From a materials science perspective this involves the identification of the transport pathways through a composite material

containing two inorganic phases embedded in an organic polymer network. There are two major aspects to this activity including (i) the materials science of the system and (ii) the limits of the tomographic approach to detect structures of importance to the materials science.

4.1. Materials Science

Transport within inhibited epoxy coatings has been of interest for some time. Spatial scales involved in transport in inhibited epoxy coatings range from the macroscopic down to close to the atomic level. At the macroscopic level (centimeters to millimeters) features such as cracks and pinholes in coatings easily allow ingress of corrodents to the substrate and egress of inhibitors from the primer/defect interface into the defect. At the submillimeter to micron scale there are a range of features that may be of importance for the transport of inhibitors from (i) the arrangement of the inhibitors particles, with themselves (clustering), (ii) arrangements with other additives which may provide "sinks" for the inhibitor if they absorb/adsorb on them and (iii) structures within the polymer itself such as density variations. The exact scale at which these features become important will depend on the sizes of the additives and their agglomerates as well as the mixing processes. At the molecular level both polymer structure and interfacial structure are important.

4.2. Physico-chemical Characterisation

From the discussion above it becomes immediately obvious that there is a range of scales where characterization is required perhaps scanning as much seven orders of magnitude (from the nanometer scale to a few hundred microns). While some techniques do provide averaged information of a sort over all these length scales *e.g.* impedance spectroscopy used to study the diffusion of agents such as water through coatings, they generally involve averaging over large areas of the coatings. Most imaging techniques are usually performed from the sub-micron scale up to the hundreds of micron scale and are performed on 2D sections that do not provide insightful data on the 3D structure.

In this later respect, X-ray tomography is probably one of the most useful techniques for structural characterization for epoxy coatings containing additives since it spans three orders of magnitude to cover some of the most important structural scales for these systems. In this study the size distribution of clusters of TiO_2 and $SrCrO_4$ particles were determined before and after leaching. In this respect, $SrCrO_4$ particles and clusters were investigated at scales from 3.5 μm to the millimeter scale. The leaching experiments revealed that the number and total voxel count of the $SrCrO_4$ clusters was reduced from 2828 and 788739 respectively to 1210 and 571477 respectively representing a 28% reduction in $SrCrO_4$. There was no detectable change in the TiO_2 content as it is not soluble under the leaching conditions. The void and polymer density fluctuations were also monitored. In the latter case X-Ray absorption contrast may be the only technique capable of imaging density differences in polymers. The increase in this combined component reflects the loss of $SrCrO_4$ (dissolution creating void), but the increase in the level of connection to the external surface (Figure 7(right)) provides an explanation for the release of chromate.

Despite the successful quantification of the $SrCrO_4$ component there are still challenges. The $SrCrO_4$ and TiO_2 particles in the sample are small in physical size and have much higher X-ray linear absorption coefficients than the polymer matrix. The phase-contrast and the point-spread-function effects cause difficulties in reconstructing their linear absorption coefficient maps. On the other hand,

the X-ray attenuation contrast between the polymer matrix, LDE and void fall within the X-ray CT noise level. X-ray radiation damage to the polymer matrix during the imaging process has added additional artefacts to the images. Refined experimental design and theoretical analysis to minimize the effect of above factors are in progress.

5. Conclusion

In this paper a comparison of an inhibited primer coating before and after leaching has been made. The primer consisted of TiO_2 and $SrCrO_4$ particles embedded in an epoxy matrix. The sample shape was a cylinder. From the tomographic studies the size distributions of TiO_2 and $SrCrO_4$ clusters were determined and revealed that, after leaching, the $SrCrO_4$ clusters distribution changed significantly showing that clusters of all sizes were removed from the sample. The total change in volume of the $SrCrO_4$ particles was 28%. The TiO_2 distribution remained unchanged. The void and low density epoxy components also increased presumably through the addition of void resulting from the dissolution of the $SrCrO_4$ clusters. These results suggest that the leaching pathway for the dissolved $SrCrO_4$ was through the void and low density pathways.

Conflict of Interest

There is no conflict of interest related to this document.

References

1. Hughes A, Trinchi A, Chen F, et al. (2014) Revelation of Intertwining Organic and Inorganic Fractal Structures in Polymer Coatings. *Adv Mater* 26: 4504–4508.
2. Hughes A, Trinchi A, Chen F, et al. (2014) The application of multiscale quasi 4D CT to the study of $SrCrO_4$ distributions and the development of porous networks in epoxy-based primer coatings. *Prog Org Coat* 77: 1946–1956.
3. Trueman A, Knight S, Colwell J, et al. (2013) 3-D tomography by automated in situ block face ultramicrotome imaging using an FEG-SEM to study complex corrosion protective paint coatings. *Corros Sci* 75: 376–385.
4. Mookhoek S, Mayo S, Hughes A, et al. (2010) Applying SEM-Based X-ray microtomography to observe self-healing in solvent encapsulated thermoplastic materials. *Adv Eng Mater* 12: 228–234.
5. Müller B, Lange A, Harwardt M, et al. (2009) Synchrotron-based micro-ct and refraction-enhanced micro-ct for non- destructive materials characterisation. *Adv Eng Mater* 11: 435–440.
6. Desrues J, Viggari G, Besuelle P (2006) *Advances in X-ray Tomography for Geomaterials* ,ISTE, London.
7. Yang S, Gureyev T, Tulloh M, et al. (2010) Feasibility of a data constrained prediction of hydrocarbon reservoir sandstone microstructures. *Meas Sci Technol* 21: 047001.
8. Yang S, Gao D, Muster T, et al. (2010) Microstructure of a paint primer—a data-constrained modeling analysis. *Pricm 7, Pts 1-3*, edited by J. F. Nie and A. Morton (2010) 654–656: 1686–1689.

9. Mayo S, Tulloh A,Trinchi A, et al. (2012) Data-constrained microstructure characterization with multispectrum x-ray micro-ct. *Microsc Microanal* 18: 524–530 .
10. Wang H, Yang Y, Yang J, et al. (2015) Evaluation of Multiple-Scale 3D Characterization for Coal Physical Structure with DCM Method and Synchrotron X-Ray CT. *Scientific World J* 2015: 414262.
11. Yang Y, Tulloh A, Muster T, et al. (2010) Data constrained microstructure modelling with multi-spectrum X-ray CT. *P SPIE OpticsPhotonic* 7804: 7804N.
12. Yang Y, Chu C. DCM – A software platform for 3D material microstructure characterisation, properties modelling & visualisation. Available from: http://research.csiro.au/dcm.
13. Gureyev T, Nesterets Y, Ternovski D, et al. (2011) in *Toolbox for advanced x-ray image processing*. 81410B.
14. Paganin D, Mayo S, Gureyev T, et al. (2002) Simultaneous phase and amplitude extraction from a single defocused image of a homogeneous object. *J Micros Oxford* 206: 33–40.
15. Yang Y, Liu K, Mayo S, et al. (2013) A data-constrained modelling approach to sandstone microstructure characterization. *J Pet Sci Eng* 105: 76–83.
16. Yang Y, Tulloh A, Chen F, et al. (2013) Data-constrained characterization of sandstone microstructures with multi-energy X-ray CT. *J Phy Conf Ser* 463: 012048.
17. Wang H, Yang Y, Wang Y, et al. (2013) Data-constrained modelling of an anthracite coal physical structure with multi-spectrum synchrotron X-ray CT. *Fuel* 106: 219–225.
18. Yang Y, Tulloh A, Chu C, et al. DCM - A Software Platform for Advanced 3D Materials Modelling, Characterisation and Visualization. *CSIRO Data-Access-Portal*. Available from: https://data.csiro.au/dap/landingpage?pid=csiro:9448.
19. Yang Y (2012) A data-constrained non-linear optimisation approach to a data-constrained model for compositional microstructure prediction. *Lect Notes Inform Technol* 15: 198–205.
20. Sellaiyan S, Hughes A, Smith S, et al. (2014) Leaching properties of chromate-containing epoxy films using radiotracers, PALS and SEM. *Prog Org Coat* 77: 257–267.

AIMS Press